Numerical Simulations of Lateral Dispersion by the Relaxation of Diapycnal Mixing Events

MILES A. SUNDERMEYER

School for Marine Science and Technology, University of Massachusetts—Dartmouth, New Bedford, Massachusetts

M.-PASCALE LELONG

NorthWest Research Associates, Bellevue, Washington

(Manuscript received 15 March 2004, in final form 6 June 2005)

ABSTRACT

In this second of two companion papers, numerical simulations of lateral dispersion by small-scale geostrophic motions, or vortical modes, generated by the adjustment of mixed patches following diapycnal mixing events are examined. A three-dimensional model was used to solve the Navier–Stokes equations and an advection/diffusion equation for a passive tracer. Model results were compared with theoretical predictions for vortical mode stirring with results from dye release experiments conducted over the New England continental shelf. For "weakly nonlinear" cases in which adjustment events were isolated in space and time, lateral dispersion in the model was consistent to within a constant scale factor with the parameter dependence

$$\kappa_H \propto \left(\frac{1}{2}\right)\left(\frac{h^4\Delta N^4}{L^2 f^4}\right)\phi\left(\frac{h^2/\nu_B}{1/f}\right)$$

predicted by Sundermeyer et al., where h and L are the vertical and horizontal scales of the mixed patches, ΔN^2 is the change in stratification associated with the mixed patches, f is the Coriolis parameter, ϕ is the frequency of diapycnal mixing events, and ν_B is the background viscosity. The associated scale factor, assumed to be of order 1, had an actual value of about 7, although this value will depend, in an unknown way, on the assumed horizontal scale of the mixed patches, which was here held constant at close to the deformation radius. A second more energetic parameter regime was also identified in which vortical mode stirring became strongly nonlinear and the effective lateral dispersion was larger. Estimates of the relevant parameters over the New England shelf suggest that this strongly nonlinear regime is more relevant to the real ocean than the weakly nonlinear regime, at least under late summer conditions. This suggests that stirring by small-scale geostrophic motion may, under certain conditions, contribute significantly to lateral dispersion on scales of 1–10 km in the ocean.

1. Introduction

Analysis by Sundermeyer (1998) and Sundermeyer and Ledwell (2001) of a series of tracer release experiments conducted during late summer stratification over the New England continental shelf has shown that isopycnal dispersion on scales of 1–10 km and periods of 1–5 days cannot be explained by existing models of lateral dispersion—namely, shear dispersion and dispersion by interleaving water masses. A similar result was found by Ledwell et al. (1998) and Sundermeyer and Price (1998) in relation to the North Atlantic Tracer Release Experiment in the pycnocline of the open ocean; in that case, internal wave shear dispersion could not account for dispersion on scales of a few tens of kilometers and periods of a few weeks. One explanation for this discrepancy, proposed by Sundermeyer (1998) and Sundermeyer et al. (2005) in relation to dye release experiments performed over the New England shelf and by Polzin and Ferrari (2004) in relation to the open ocean, is that the observed lateral dispersion on scales of 1–10 km may be explained by the presence of

Corresponding author address: Miles A. Sundermeyer, School for Marine Science and Technology, University of Massachusetts—Dartmouth, 706 Rodney French Blvd., New Bedford, MA 02744-1221.
E-mail: msundermeyer@umassd.edu

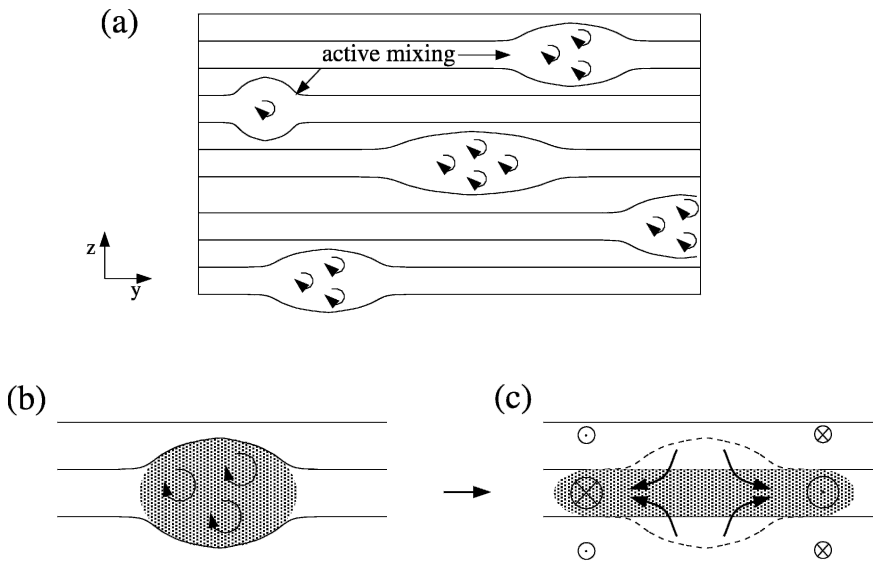

FIG. 1. (a) Schematic of the adjustment of diapycnal mixing events and the formation of small-scale geostrophic motions, or vortical modes. Horizontal lines represent isopycnals, with lenses of well-mixed fluid superimposed. (b), (c) A single mixing event and the ensuing lateral spreading during the adjustment. [Reprinted with permission from Sundermeyer and Ledwell (2001), copyright by the American Geophysical Union.]

submesoscale geostrophic motions, or vortical modes, generated by the adjustment of mixed patches following diapycnal mixing events (e.g., Kunze 2001). In the coastal ocean, Sundermeyer et al. (2005) hypothesized that a random field of vortical modes could cause sufficient stirring on these scales to efficiently disperse a dye patch. In the open ocean it is possible that vertical shear dispersion associated with the vertical structure of the vortical modes may also be important, although Sundermeyer et al. (2005) suggest this is unlikely.

In the present study, we use a numerical model to simulate the adjustment of mixed patches of fluid following diapycnal mixing events and test the hypothesis that lateral dispersion caused by the resulting small-scale geostrophic motion, or vortical modes, may lead to significant dispersion on scales of 1–10 km in the ocean. In particular, we focus on testing the parameter dependence proposed by Sundermeyer et al. (2005) for scales relevant to the coastal ocean. A companion paper by Lelong and Sundermeyer (2005, henceforth LS) examines the relaxation of a single diapycnal mixing event and its effect on lateral dispersion.

a. Overview of vortical mode stirring

The process of lateral dispersion by small-scale vortices caused by patchy mixing relies on the fact that diapycnal mixing in the ocean is not uniform in space and time. Rather, it is episodic, consisting of isolated events that are the result of breaking internal waves (e.g., Phillips 1966; Garrett and Munk 1972). The result of episodic mixing is that localized regions of weak stratification are generated preferentially in regions of intense mixing. These low stratification regions result in local horizontal pressure gradients that cause the well-mixed fluid to adjust laterally, forming "blini," or "pancakes" (Fig. 1) (Phillips 1966). The process of adjustment may lead to two types of motions: a slumping velocity directed radially outward and, in the case of geostrophic adjustment, an azimuthal velocity that is geostrophically balanced. For both types of motions, the net effect of the adjustment is the same; fluid will be displaced laterally. However, of particular interest here are the geostrophically balanced motions since they can persist for much longer times. For a single event, the lateral displacement is appropriately described as an advective process. However, for a large number of events, the sum of the displacements can be thought of as a random walk with rms step size equal to the rms horizontal displacement averaged over the events, that is, an effective lateral diffusivity.

The hypothesis that vortical mode stirring may be important in the coastal ocean is based on results from dye release experiments and microstructure observations made during the Coastal Mixing and Optics Experiment (CMO) (Sundermeyer and Ledwell 2001; Ledwell et al. 2004; Oakey and Greenan 2004). Analysis by Sundermeyer and Ledwell (2001) of the lateral dispersion during these experiments showed that the

observed dispersion could not be explained by shear dispersion or lateral intrusions. In addition, in all of the experiments they observed patchiness in the dye distributions 6–12 h after injection. Horizontal and vertical transects through the dye suggest that the patchiness occurred on scales of 0.5–10 m vertically and a few hundred meters to a few kilometers horizontally. This combined with the short time it took the dye to evolve from a single coherent streak to a more convoluted/patchy distribution suggest the presence of some stirring mechanism at these scales.

In addition to the dye observations, concurrent temperature and velocity microstructure observations during CMO also showed significant patchiness (Oakey and Greenan 2004; Sundermeyer et al. 2005). Specifically, microstructure transects showed localized regions of intense mixing superimposed on a relatively quiescent background of low diapycnal diffusivities. These regions of high mixing, which were ubiquitous throughout the data, had vertical scales ranging from 2 to 10 m and horizontal scales ranging from a few hundred meters to a few kilometers. Furthermore, as shown by Sundermeyer et al. (2005), at least some of the microstructure patches were strong enough and long lived enough to induce $O(1)$ changes in stratification. Both the dye and microstructure observations were thus consistent with the hypothesis that the observed stirring of the tracer patch may have been caused by small-scale motions following diapycnal mixing events.

b. Scope and outline

While the adjustment of mixed patches may not be the only source of vortical mode energy in the ocean, in the present study, we focus on this mechanism as a pathway to lateral stirring. The scaling results of Sundermeyer (1998) and Sundermeyer et al. (2005) provide order-of-magnitude estimates of the effectiveness of stirring by this process. However, these scaling have not yet been quantitatively tested; a more precise prediction that includes a fuller description of the physics is needed. The present study attempts to provide such a description by examining numerically the effects of vortical mode stirring on a passive tracer.

We concentrate here on scales relevant to the coastal ocean, specifically those relevant to the CMO study site. For reasons that will soon become apparent, however, we limit our analysis to cases in which diapycnal mixing events are relatively infrequent, and hence the vortical mode field is, as we shall argue, considerably less energetic than in the real ocean. In addition, to balance the trade-off between numerical tractability and geophysical realism, we employ two numerical techniques to simplify our computations. First, we artificially increase the Coriolis frequency in our model by an order of magnitude so as to reduce the ratio of the buoyancy frequency to the Coriolis frequency, N/f. This allows us to resolve internal wave motions while still integrating over the many hundreds of inertial periods required for model spinup. Second, we use both Newtonian and hyperviscosities in our model. The former provides a tunable viscosity parameter, while the latter ensures computational stability. With these modifications (see sections 3 and 4 for more details) our goal is to provide a first look at how the adjustment of mixed patches affects lateral dispersion in the ocean and how this dispersion depends on external parameters. We then relate our findings back to realistic ocean parameter space and comment on the implications of our results to the coastal ocean.

The remainder of this paper is organized as follows. In section 2 we review the geostrophic/random walk scaling of Sundermeyer (1998) and Sundermeyer et al. (2005). Section 3 describes the numerical model. In section 4 we describe the parameters used in a base case model run. Also in section 4, we investigate the dependence of κ_H on relevant model parameters. In section 5, we discuss the implications of our results. Section 6 provides a brief summary and concludes.

2. Theoretical background

a. Momentum balance

As a first test to determine whether small-scale vortices caused by patchy mixing could explain lateral diffusivities observed during CMO, Sundermeyer (1998) and Sundermeyer et al. (2005) used scale analysis applied to the horizontal momentum equations combined with a simple random walk formulation to obtain order of magnitude estimates of the effective lateral dispersion due to the adjustment of mixed patches following diapycnal mixing events. Specifically, they considered term balances in the x component of the horizontal momentum equation,

$$\frac{\partial u}{\partial t} + \mathbf{u}\cdot\nabla u - fv = -\frac{1}{\rho}\frac{\partial P}{\partial x} + \nu_B \frac{\partial^2 u}{\partial z^2}, \qquad (1)$$

where all variables have their traditional meanings and ν_B represents some ambient background viscosity, which may be either molecular or eddy viscosity representing processes outside the mixing events themselves. Scaling this equation, it follows that

$$\left(\frac{U}{T}\right)\left(\frac{U^2}{L}\right)(fU)\left(\frac{h^2}{L}\Delta N^2\right)\left(\nu_B \frac{U}{h^2}\right), \qquad (2)$$

where U and L represent horizontal velocity and length scales, respectively; T is a characteristic time scale; h is the vertical scale of the mixing events; ΔN^2 is the change in stratification associated with the events; and the scaling for the pressure gradient term has been obtained from the hydrostatic equation. The latter derives from taking $\partial/\partial z$ of the hydrostatic equation,

$$\frac{\partial}{\partial z}\frac{\partial P}{\partial z} = -g\frac{\partial \rho}{\partial z} = N^2\rho_o, \tag{3}$$

and noting that P scales as $N^2h^2\rho_o$. Substituting this into the x-momentum equation and further noting that $N^2 = N^2_{\text{background}} + \Delta N^2$, it follows that the horizontal pressure gradient term in (2) scales as $\Delta N^2h^2/L$. (Note that $\partial P/\partial x$ gives ΔN^2 rather than total N^2 since the background stratification is assumed to be constant over the scale of the mixed patch.) Last, dividing (2) through by fU gives the equivalent nondimensional form,

$$\left(\frac{1}{fT}\right)(\text{Ro})(1)\left(\frac{\text{Bu}}{\text{Ro}}\right)(\text{Ek}), \tag{4}$$

where $\text{Bu} = (h^2\Delta N^2)/(f^2L^2)$ is the Burger number, $\text{Ro} = U/(fL)$ is the Rossby number, and $\text{Ek} = \nu_B/(h^2f)$ is the Ekman number. [Note, Sundermeyer et al. (2005) unconventionally defined the Ekman number as the inverse of this last quantity. To avoid confusion here, whenever we mean h^2f/ν_B, we will use the term inverse Ekman number.]

The above expressions represent the basic momentum balance associated with the relaxation and adjustment following diapycnal mixing events. Assuming patches of mixed fluid adjust geostrophically, which based on the relevant time and space scales estimated by Sundermeyer et al. (2005) appeared to have been the case during CMO, we envision a classic Rossby adjustment problem. The buoyancy anomaly induced by diapycnal mixing results in a horizontal pressure gradient as represented by the first term on the rhs of (1). If the anomaly is rotationally symmetric in the horizontal and if the influence of friction is small, this pressure gradient leads to an initial radial spreading of the well-mixed fluid of order the deformation radius. As this initial adjustment occurs, a geostrophic flow is established in the azimuthal direction such that the mixed region rotates anticyclonically. Geostrophic adjustment is not the only possible scenario; ageostrophic adjustment may also occur (Sundermeyer et al. 2005). However, here we focus on the geostrophic adjustment regime.

b. Geostrophic/random walk scaling

The theoretical scaling of Sundermeyer et al. (2005) provides a first estimate of how the effective diffusivity by small-scale vortices caused by patchy mixing might vary with key parameters. They showed that, for a series of mixing events and for a given vertical diffusivity, there exists an optimal scale of mixing events for which a maximum effective horizontal diffusivity results. This maximum diffusivity is predicted to occur when the horizontal scales of mixing events are comparable to the internal deformation radius, $R = h\Delta N/f$, and the vertical scales are large enough that events adjust geostrophically. In that case, the horizontal velocity U associated with the adjustment of the well-mixed fluid scales as

$$U \approx \frac{h^2\Delta N^2}{Lf}, \tag{5}$$

where L is the horizontal scale of the mixing event. Assuming the displacement associated with this adjustment represents a step in a horizontal random walk and that the step size S is given by the geostrophic velocity times the adjustment time scale, $T = 1/f$, they proposed that the step size can be expressed as

$$S = UT \approx \frac{h^2\Delta N^2}{Lf^2} = \frac{R^2}{L}. \tag{6}$$

Writing the effective horizontal diffusivity as the step size squared times the frequency of events, ϕ (i.e., the frequency of taking a step), it follows that the effective horizontal diffusivity scales as

$$\kappa_H \approx \left(\frac{1}{2}\right)S^2\phi \approx \left(\frac{1}{2}\right)\frac{h^2\Delta N^4}{L^2f^4}\,\phi. \tag{7}$$

Last, assuming that the buoyancy flux associated with an ensemble of mixing events can be expressed in terms of a diapycnal diffusivity, κ_z (e.g., Garrett and Munk 1972; Vanneste and Haynes 2000), that is, approximately,

$$\kappa_z = \frac{1}{3}\frac{\Delta N^2}{N^2}h^2\phi, \tag{8}$$

and substituting for ΔN^2h^2 in terms of κ_z, and for the deformation radius, $R = \Delta Nh/f$, they showed that the effective horizontal diffusivity in (7) can be equivalently expressed as

$$\kappa_H \approx \left(\frac{3}{2}\right)\left(\frac{N^2}{f^2}\right)\left(\frac{R^2}{L^2}\right)\kappa_z. \tag{9}$$

As discussed by Sundermeyer et al. (2005), the above expression for the effective lateral dispersion by small-scale vortices, or vortical modes, caused by patchy mixing is likely to be low for the following reasons. First, the above scaling uses an inertial time scale, $T = 1/f$, to

estimate the displacement associated with an individual event. However, it is likely that longer-lived vortices will continue to displace fluid and contribute to stirring for many inertial periods until they are eventually dissipated away (see also LS). Although the stirring efficiency of any individual vortex likely diminishes after many eddy rotation periods (as nearby fluid becomes mixed), for inverse Ekman numbers of order 10 or less Sundermeyer et al. (2005) argued that the contribution of a given vortex to lateral stirring should still scale as the diffusion time scale divided by the inertial period, fh^2/ν_B; hence, (7) and (9) become

$$\kappa_H \approx \left(\frac{1}{2}\right) S^2 \phi\left(\frac{h^2/\nu_B}{1/f}\right) \approx \left(\frac{1}{2}\right) \frac{h^4 \Delta N^4}{L^2 f^4} \phi\left(\frac{h^2/\nu_B}{1/f}\right) \quad (10)$$

and

$$\kappa_H \approx \left(\frac{3}{2}\right)\left(\frac{N^2}{f^2}\right)\left(\frac{R^2}{L^2}\right)\left(\frac{h^2/\nu_B}{1/f}\right)\kappa_z. \quad (11)$$

If the diffusion time scale is equal to one inertial period, then $fh^2/\nu_B = 1$, and (10) and (11) revert to (7) and (9). However, if $fh^2/\nu_B > 1$, then κ_H will increase proportionally, as each additional inertial period that a given anomaly contributes to stirring is akin to taking an additional step. While successive "steps" due to a given anomaly may become progressively less effective in comparison with the initial displacements (since no new fluid is being advected), as we shall show in our numerical simulations, this effect is limited, at least for inverse Ekman number of order 10 or less.

A second reason that the above estimates of κ_H may be low is that they do not explicitly account for nonlinear interactions between vortices; rather, they assume that each step occurs in isolation. The above formulation therefore does not account for strongly nonlinear interactions between vortices or for vortex merging, both of which can have significant effects on the energy-containing scales and, hence, can alter the effective horizontal diffusivity, κ_H. Neither is this effect accounted for by the addition of the diffusive time scale, fh^2/ν_B, although the latter at least takes into account the lifetime of individual vortices.

3. Model description

The major goal of this paper is to test the above theoretical ideas for vortical mode stirring as they may apply to the ocean. To this end, we have incorporated into a numerical model the relevant dynamics of the adjustment of mixed patches following diapycnal mixing events, and the resulting lateral dispersion.

a. Governing equations

We used a fully optimized and parallelized code developed by Winters et al. (2004) to solve the three-dimensional *f*-plane Boussinesq equations and an advection/diffusion equation for a passive tracer, whose concentration is denoted by C. The model equations were solved spectrally on a triply periodic domain:

$$\frac{D\mathbf{u}}{Dt} + f\mathbf{i}_3 \times \mathbf{u} = -\frac{1}{\rho_o}\boldsymbol{\nabla} P - \mathbf{i}_3 \frac{g}{\rho_o}\rho + \nu_2\nabla^2\mathbf{u} + \nu_6\nabla^6\mathbf{u}, \quad (12)$$

$$\boldsymbol{\nabla}\cdot\mathbf{u} = 0, \quad (13)$$

$$\frac{D\rho}{Dt} = \kappa_2\nabla^2\rho + \kappa_6\nabla^6\rho, \quad \text{and} \quad (14)$$

$$\frac{DC}{Dt} = \kappa_2\nabla^2 C + \kappa_6\nabla^6 C, \quad (15)$$

where all variables have their traditional meanings. Noteworthy in our implementation of the model, however, is our use of both Newtonian viscosity and diffusivity, represented respectively by ν_2 and κ_2, and hyperviscosity and hyperdiffusion, represented by ν_6 and κ_6. While the former are physically motivated, the latter are strictly numerical inasmuch as they were designed to affect the smallest scales in both horizontal and vertical directions in a manner independent of grid resolution. The latter is achieved by normalizing the hyperviscosity by the maximum nondimensional wavenumber in the relevant coordinate direction; that is, $\nu_6 = \nu_6'/k_{\max}^6$, where ν_6' is the more familiar hyperviscosity. For grid resolutions of nx = nz = 64 for example, the horizontal and vertical normalization factors are $k_{\max}^6 = 208$ and 5.4×10^{13}, respectively. This approach, combined with the wavenumber truncation method of Patterson and Orszag (1971), is used to dissipate energy and tracer variance at the smallest scales. In practice, we use the ∇^6 viscosity and diffusion to ensure computational stability, while the ∇^2 terms represent background viscosity and diffusivity, ν_B and κ_B [e.g., see Eq. (1)], respectively, adjusted based on dynamical considerations. Note that, for most of the runs reported here, the Newtonian viscous time scale is much shorter in the vertical direction than in the horizontal direction because of the small aspect ratio of the model domain. Furthermore, hyperviscosity is important at only the very smallest scales in both the vertical and horizontal.

b. Model setup

Except where otherwise noted, the simulations described here used 64 grid points in the vertical, and

TABLE 1. Model parameters for the base run.

Variable	Symbol	Model value	Scaled value
Horizontal and vertical domain size	$L_x = L_y$, L_z	500 m, 12.5 m	5 km, 12.5 m
Coriolis parameter	f	9.5×10^{-4} s^{-1}	9.5×10^{-5} s^{-1}
Background stratification	$\partial\rho/\partial z$	0.037 kg m^{-4}	0.037 kg m^{-4}
Interval between anomalies	T_ϕ	$2707 \times 2\pi/f$	$2707 \times 2\pi/f$
Anomaly amplitude	$\Delta N^2/N^2$	1.0	1.0
Anomaly horizontal scale	$L = 2\sigma_x$, $2\sigma_y$	50 m	500 m
Anomaly vertical scale	$h = 2\sigma_z$	1.25 m	1.25 m
∇^2 viscosity	ν_2	2.5×10^{-5} m^2 s^{-1}	2.5×10^{-6} m^2 s^{-1}
∇^2 diffusivity	κ	2.5×10^{-6} m^2 s^{-1}	2.5×10^{-7} m^2 s^{-1}
∇^6 viscosity (horizontal)	ν_6	48 m^6 s^{-1}	—
∇^6 diffusivity (horizontal)	κ_6	48 m^6 s^{-1}	—
∇^6 viscosity (vertical)	ν_6	1.8×10^{-10} m^6 s^{-1}	—
∇^6 diffusivity (vertical)	κ_6	1.8×10^{-10} m^6 s^{-1}	—
Model time step	Δt	30 s	30 s
Total model run time	—	$800 \times 2\pi/f$	$800 \times 2\pi/f$
Tracer injection time	—	$100 \times 2\pi/f$	$100 \times 2\pi/f$

either (64 × 64) or (128 × 128) grid points in the horizontal. A number of higher-resolution runs were also conducted using (128 × 128 × 128) and (256 × 256 × 128) grid points. Typical horizontal and vertical domain sizes were $L_x = L_y = 500$ m (equivalently $L_x = L_y = 5000$ m after N/f scaling; see section 3*e* below and also LS), and $L_z = 12.5$ m, respectively. These scales were chosen based on observational results, as well as considerations of computational stability and tractability. Specifically, Sundermeyer et al. (2005) estimated the deformation radius associated with mixed patches over the New England shelf to be approximately $R = 325$ m. A horizontal domain of 5000 m thus can accommodate multiple anomalies across the domain, while avoiding self-interaction of individual anomalies across the model's periodic boundaries. The latter conditions are necessary so that multiple anomalies within the model domain behave as a (quasi) random field of eddies rather than as an array of regularly spaced eddies across the models periodic boundary conditions. Meanwhile, in the vertical, Sundermeyer et al. (2005) estimated that the scales of mixing events ranged from about 1 to 10 m. In most of our simulations we thus used mixing events of vertical scale $h = 1.25$ m since larger vertical scales would have necessitated even shorter integration time steps. Analogous to the horizontal, this also allowed multiple anomalies in the vertical without self-interaction across the model's periodic vertical boundaries.

c. Initial conditions and forcing

To simulate lateral stirring by vortical motions, the model was spun up from a state of rest and uniform stratification by injecting potential energy (PE) in the form of randomly placed Gaussian-shaped stratification anomalies. This was done by periodically imposing a short-lived Gaussian diffusivity profile of the form

$$\kappa_z(x, y, z, t) = \frac{1}{\Delta t}\frac{\Delta N^2}{N^2} z_o^2 \exp\left(-\frac{x^2}{2\sigma_x^2} - \frac{y^2}{2\sigma_y^2} - \frac{z^2}{2\sigma_z^2} \right), \tag{16}$$

at random locations in the model in the manner described by LS. Here we choose the variances σ_x, σ_y, and σ_z to be at least 1/20 of the overall model domain so that, for example, in a 64-gridpoint domain, a Gaussian anomaly profile of width 4σ would be represented by at least 13 grid points in any coordinate direction (Table 1). The imposed diapycnal diffusivity was applied to all dynamical variables, namely, u, v, w, ρ, and C. The resulting stratification anomalies were then allowed to freely adjust to form small-scale vortical motions plus internal waves. This forcing was intended to represent episodic mixing events caused by a random internal wave breaking. We made no attempt to explicitly simulate the turbulent mixing events themselves. Rather, we parameterized their effect as randomly placed stratification anomalies, or buoyancy flux events. Using this approach, the model was spun up to a statistically stationary state in which the input of PE and subsequent conversion to kinetic energy (KE) was balanced by dissipation.

d. Model tracer/inferred κ_H

Passive tracer was released into the model once the flow reached a statistical equilibrium. The initial condition for the tracer was a Gaussian streak at the center

of the domain oriented with its major axis in the y-coordinate direction:

$$C(x, y, z) = \exp\left(-\frac{x^2}{2\sigma_x^2} - \frac{z^2}{2\sigma_z^2} \right). \tag{17}$$

This configuration allowed us to evaluate lateral dispersion in the x and z directions, but not the y direction. Note, however, that, since the model is homogeneous and isotropic in x and y, the latter did not pose any limitation to our analysis; it merely allowed us to diagnose horizontal mixing coefficients more efficiently.

To ensure that the tracer streak was at least initially well resolved in the model, we used the same σ_x and σ_z in (17) as for the density anomalies in (16), namely 1/20 of the model domain. Although this choice of tracer scales also fixes the scale of the tracer patch relative to the anomaly scale, this does not effect our results since it is the longer-term dispersion acting over the scale of the domain that determines the lateral diffusivity, in which we are interested, and this long-term dispersion is insensitive to the initial condition after a relatively short time. An additional advantage of maintaining the scale of the dye patch relative to the scale of the anomalies is that, when model runs are dynamically similar, this similarity is also readily apparent in the dye fields.

Effective vertical and horizontal diffusivities in the model were diagnosed by estimating the time rate of change of the second moment of tracer in the z and x directions, respectively. For example, in the x direction

$$\kappa_H = \frac{1}{2}\frac{\partial \sigma_x^2}{\partial t}, \tag{18}$$

where

$$\sigma_x^2 = \frac{\displaystyle\int_0^{L_x} x^2 C\, dx - \left(\int_0^{L_x} xC\, dx \right)^2}{\displaystyle\int_0^{L_x} C\, dx}, \tag{19}$$

and L_x is the domain size in the x direction. The expression for the vertical diffusivity is similar. In the trivial case of no diapycnal mixing events being introduced into the model, the vertical and horizontal diffusivities would be equal to the explicit diffusivity, κ_2, provided that the Fickian diffusivity term in (14) was much larger than the hyperdiffusivity term, which it was. Any diffusivity in excess of this could therefore be attributed to stirring by small-scale vortices, or vortical modes, caused by patchy mixing.

e. N/f and viscous scaling

As in LS, to keep the simulations computationally tractable the Coriolis frequency f was artificially increased by a factor of 10 relative to realistic values in the majority of our runs. The effect of this was to reduce the ratio of the buoyancy frequency to the Coriolis frequency, N/f, from a realistic value of approximately 200 to a more tractable value of approximately 20. This allowed us to capture the dynamics associated with both of these time scales, that is, internal waves and geostrophic adjustment, without having to perform prohibitively long numerical integrations or use prohibitively small time steps. As described in LS and discussed briefly in section 4, this artificial increase in f did not fundamentally alter the dynamics of the adjustment of mixed patches or the resultant vortical mode stirring in our model, provided that two additional conditions were met. First, in the increased f runs, we also reduced the horizontal scale of the anomalies, L, so as to maintain the ratio of the size of the anomalies to the geostrophic deformation scale

$$R = \frac{\Delta N h}{f},$$

and the importance of the nonlinear advection terms in the horizontal momentum equations. In other words, considering (4), we held both the Burger number and the Rossby number fixed. This ensured that the geostrophic displacement associated with adjustment occurred on the same scale relative to the anomalies, independent of the value of f. A consequence of this reduced N/f scaling was that all horizontal scales in our model were also effectively reduced by a factor of 10. Thus, for example, a realistic horizontal domain size of $L_x = L_y = 5000$ m in our model became $L_x = L_y = 500$ m.

A second condition for dynamical similarity was that we increased viscosity/diffusion so as to hold the ratio of the diffusive time scale of the anomalies to the inertial time scale, that is, the Ekman number, fixed. The purpose of this was to maintain the relative level of importance (or unimportance) of frictional forces in both the adjustment and eventual spindown of geostrophic vortices. This meant that the molecular/subgrid-scale diffusivities in our model were also scaled relative to realistic values. Specifically, model diffusivities were of order 10 times as large as their corresponding realistic values (see discussion of viscosity parameter dependence in section 4e).

The above scalings preserve the dynamics associated with the generation and decay of vortical modes. However, as noted by LS, they do not exactly preserve the internal wave field. Nevertheless, since the internal waves do not themselves contribute significantly to lateral dispersion and since interactions between the in-

ternal wave and vortical mode fields are small, this did not significantly effect the results presented here.

Last, we note that in the analysis that follows, unless otherwise indicated, all results are reported in terms of their scaled values in order to allow direct computation of various quantities from the scaling. We shall then relate these values back to realistic values relevant to the coastal ocean in the discussion in section 5.

4. Results

a. Base parameters

To illustrate the dynamics of vortical mode stirring and to test the parameter dependence given by (10)–(11), we now present a series of model runs for a range of values of external parameters including the background stratification, N; the horizontal and vertical scales of mixing events, L and h; the change in stratification, ΔN^2; rotation, f; the frequency of mixing events, ϕ; and subgrid-scale viscosity and diffusion, ν_2 and κ_2. We begin by presenting a base model run representative of the geostrophic scaling regime described in section 2. We then examine a variety of runs in which we vary different parameters in turn and in concert in order to test the dependence of κ_H on the above variables.

Model parameters for a typical run in the geostrophic parameter regime are listed in Table 1. Values are based roughly on observations made during the CMO dye release experiments reported by Sundermeyer and Ledwell (2001) and Sundermeyer et al. (2005) except that, as described in section 3, we use an artificially increased value of the Coriolis frequency; namely, we use $f = 10 \times 2\Omega \sin(40.5°\text{N})$. Furthermore, for reasons that will be discussed later, we set the frequency of diapycnal mixing events, ϕ, to be small when compared with f. (The case of larger ϕ will be discussed in sections 4f and 5.) For realistic values of buoyancy frequency N and anomaly height h, our increased value of f decreases the deformation radius associated with the anomalies, $R = \Delta N h/f$, from 250 to 25 m. To maintain fixed Burger and Rossby numbers, we therefore also decreased the horizontal scale of the stratification anomalies from $L = 500$ m to a scaled value of $L = 50$ m. We similarly reduced the model domain size from a nominal realistic value of 5000 m to a scaled value of 500 m. Last, in order to maintain the relative importance of friction, that is, fixed Ekman number, we increased the viscosity approximately a factor of 10 from realistic values, to $\nu_2 = 2.5 \times 10^{-5}\ \text{m}^2\ \text{s}^{-1}$. Note that in order to avoid strongly nonlinear interactions in our model (see section 4f), this is slightly larger than the appropriately scaled molecular value. However, while this is true of the value used in the base run, a run with a (scaled) value similar to molecular viscosity is included in our analysis of the ν_2 parameter dependence of section 4e.

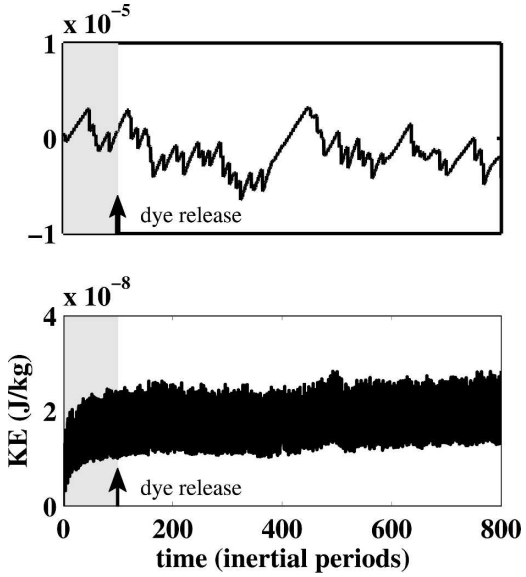

FIG. 2. Time series of (a) PE anomaly and (b) KE for a typical model run showing spinup and equilibration to a statistically steady state. Injection of model tracer is indicated by arrows and background shading. Note that negative values of the PE anomaly are an artifact of the vertically periodic boundary conditions and our method of forcing and do not represent a real extraction of PE from the system (see text).

b. Spinup and statistical equilibrium

Time series of PE and KE for the base run are shown in Fig. 2. The PE time series shows a quasi-steady level of energy modulated by the injection of anomalies over the course of the run. Note the negative values of PE are an artifact of the z periodicity in the model and the method of forcing, and do not represent a real extraction of PE from the system. This is because, although stratification anomalies strictly represent a positive buoyancy flux, anomalies injected near the top or bottom boundaries of the domain (and hence partially wrap around the domain in the vertical) appear to contribute a negative buoyancy to the total PE budget. Unfortunately, this effect masks the initial spinup of PE from $t = 0$ to the stationary equilibrium state.

The KE time series shows both the spinup from $t = 0$ and the eventual equilibration over the course of the run. Note that the time scale for spinup is of the same order as the vertical diffusion time scale for the anomalies, in this case, $T_\kappa = h^2/\kappa_2 = 100 \times 2\pi/f$. This is con-

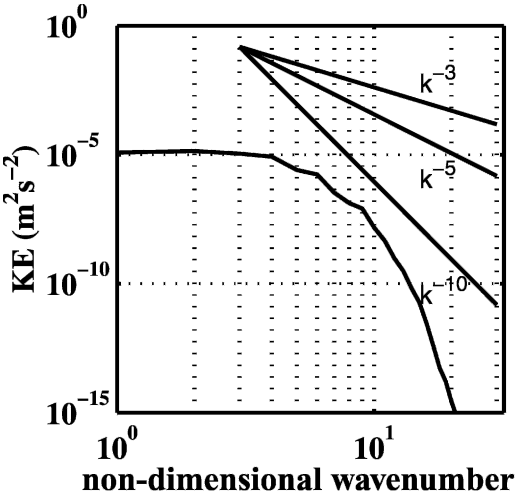

FIG. 3. Horizontal KE spectrum for a typical model run showing a spectral shape indicative of isolated vortices. The rapid decrease of energy at large wavenumber (small scales) is due to the wavenumber truncation described in the text.

sistent with the idea that the number of anomalies in the domain at any given time is determined by the diffusive time scale times the frequency of diapycnal mixing events. Closer inspection of the time series (not shown; however, see LS) further reveals that the spindown of individual anomalies is of the same order as the viscous time scale of the anomalies, $T_\nu = h^2/\nu_2 = 10 \times 2\pi/f$. This suggests that, while the KE of individual anomalies is governed by the viscous time scale, the total KE in the model is controlled by the diffusive time scale.

The horizontal KE spectrum of a fully spunup model run is shown in Fig. 3. Particularly noteworthy is the steep spectral slope, in excess of k^{-10} for large wavenumbers. A similar spectral shape was obtained for a single anomaly, except that in that case the total energy was less (see LS). This is consistent with the isolated nature of the vortices in this simulation; that is, the spectrum is simply the sum of the spectra from individual vortices and associated internal waves. Simulations in which vortices are not isolated, and therefore interact nonlinearly, give shallower spectral slopes. This case is discussed in section 4f.

c. Evolution of u, v, w, ρ, and C

Plan views and vertical cross sections of velocity, Ertel potential vorticity defined as

$$\mathrm{PV} = \left[\left(\frac{\partial v}{\partial x} - \frac{\partial u}{\partial y}\right) + f\right]\frac{N^2}{g},$$

density, and dye concentration are shown in Fig. 4. Noteworthy are the positive and negative PV anomalies in the plan views of PV corresponding to cyclonic and anticyclonic vortices formed by geostrophic adjustment following diapycnal mixing events. The presence of both positive and negative vorticity anomalies is required by conservation of PV since diapycnal mixing cannot create or destroy PV, but merely redistribute it across layers (e.g., Haynes and McIntyre 1987). Indeed this can be seen in vertical sections of PV, which show individual anomalies as anticyclonic PV cores bounded by cyclonic PV vortices above and below.

Plan views of density anomaly are similar in character to those of PV, although the details differ somewhat. Specifically, at the center of a stratification anomaly, the horizontal density anomaly is zero, while the PV is at its maximum value. This structure is best seen in vertical sections (Fig. 4), which show two-lobe structures in the density anomaly corresponding to a three-lobe structure in PV (see also LS).

Tracer distributions show the evolution of the dye from an initial Gaussian streak to one that nearly fills the domain in both the horizontal and vertical by the end of the run. Note that the horizontal deformations of the dye patch occur at the scale of the stirring vortices. Also, in the vertical, dye concentration shows significant patchiness caused by horizontal stirring at different depth levels. Last, note that, in this simulation, the rapid homogenization in the vertical is due to the explicit background diapycnal diffusivity in the model, not diapycnal mixing of episodic mixing events. This is because, in this run, we specifically chose ϕ to be small so that individual vortices did not interact with one another. A consequence of this is that the contribution of episodic mixing to the total vertical mixing is also small. As evidenced by Fig. 4, however, this does not necessarily imply that the effect on κ_H by the anomalies is small.

d. Estimates of effective diffusivities

Effective vertical and horizontal diffusivities in the model were diagnosed from the growth rate of the second moment of tracer in the horizontal and vertical using (18) and its vertical analog (Fig. 5). The resulting vertical diffusivity for the base run was $\kappa_z = 2.5 \times 10^{-6}$ $\mathrm{m^2\,s^{-1}}$, which, as expected, was the same value as the explicit Laplacian diffusivity set in the model (see Table 1). This shows that, as noted above, the net vertical diffusivity in the model was set by the explicit background diffusivity κ_z, not by event mixing. This is consistent with the fact that mixing events are relatively infrequent in our model in comparison with realistic ocean conditions (see also section 5).

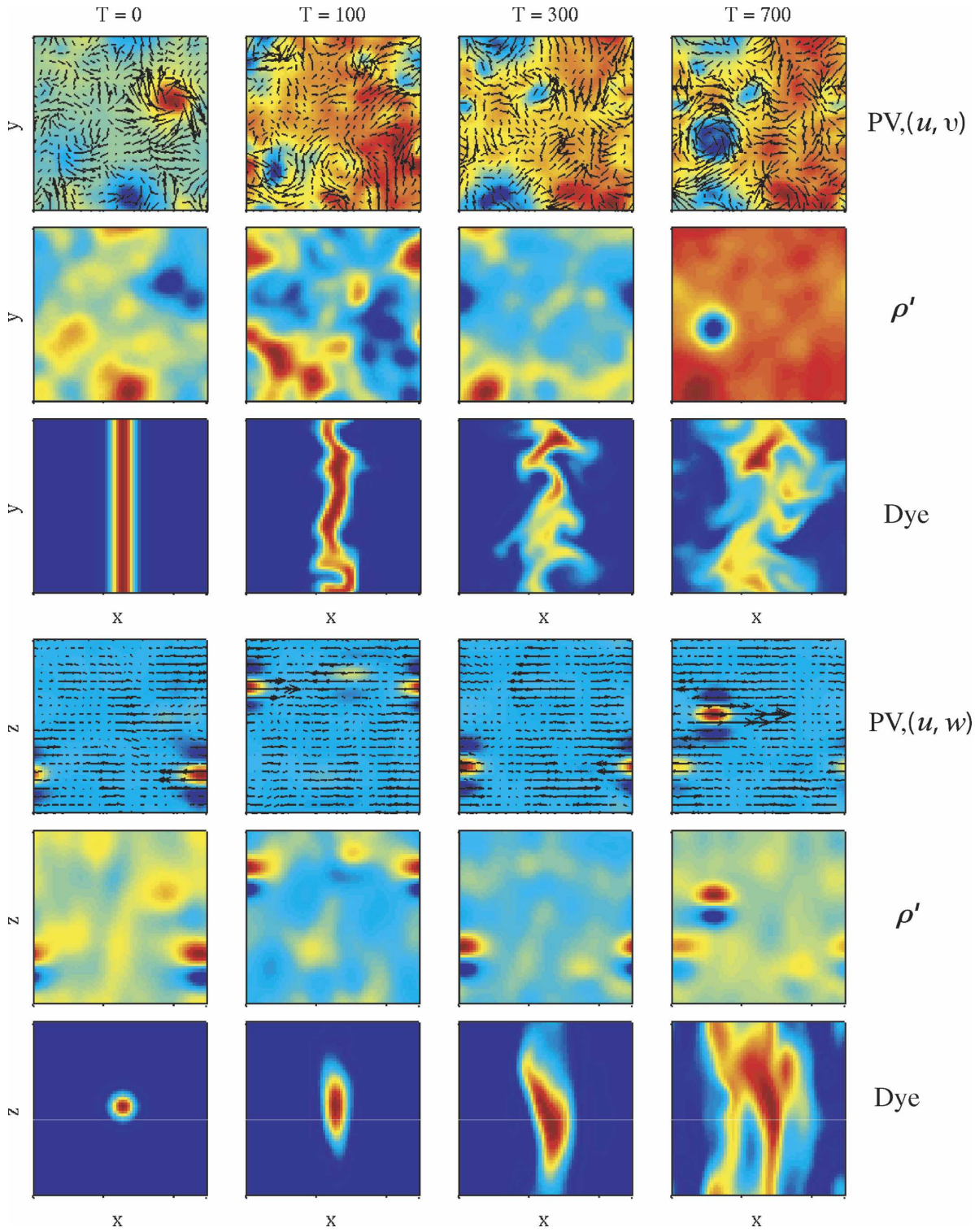

FIG. 4. Rows from top to bottom: Plan views of 1) Ertel PV with (u, v) velocity vectors overlaid, 2) density anomaly, 3) dye concentration, vertical slices of 4) Ertel PV with (u, w) velocity vectors overlaid, 5) density anomaly, and 6) dye concentration. Time increases from left to right in each row and is given in terms of number of inertial periods at the top of the figure. Domain size is 500 m $\times$ 500 m in plan view and 500 m $\times$ 12.5 m in vertical cross section.

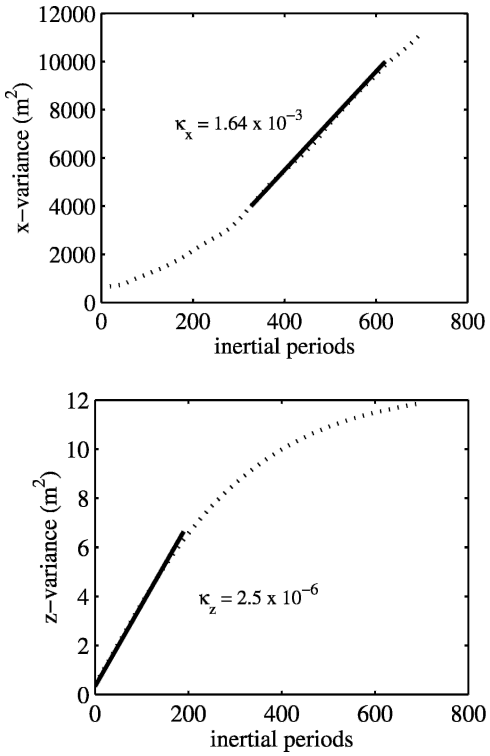

FIG. 5. Growth of second moments of model tracer in (a) the x direction and (b) z direction. Dotted lines represent the second moments defined by (18), while solid lines indicate the maximum slope, i.e., the maximum diffusivity. The asymptotic behavior for large times in the σ_z is a numerical artifact of model tracer extending across the model domain in the vertical direction.

The effective horizontal diffusivity diagnosed from model tracer in the x direction was $\kappa_H = 1.6 \times 10^{-3}$ m^2 s^{-1} (Fig. 5). This was two orders of magnitude larger than the explicit horizontal diffusivity set in the model and was clearly the result of lateral stirring, not subgrid-scale diffusive processes alone (see also Fig. 4). In comparing this value to the scaling predictions of section 2a, the actual horizontal diffusivity in the model was about 400 times that predicted by (7) and (9) and about 7 times (10) and (11). As we shall now show, this factor was approximately the same for all runs examined here. This is an importance result of this study; it suggests that the effective horizontal diffusivity predicted by Sundermeyer et al. (2005) holds to within an unknown constant scale factor and that, for the parameter range examined here, the value of the factor in (10) and (11) is approximately 7.

e. Parameter dependence: ϕ, L, h, N, f, and ν_2

To determine the dependence of κ_H on relevant forcing parameters, we next varied the different parameters on the right-hand side of (10) and (11) and examined their effect on the effective horizontal diffusivity in the model. In choosing what parameter combinations to examine, numerous factors were taken into consideration including the complexity and high order of the parameter dependence in (10) and (11), the interdependence of many of the parameters on the right-hand side of (11), and computational limitations (domain size traded off with integration time).

Event frequency (ϕ): We began with the simplest parameter dependence found in (10), that is, the frequency of diapycnal mixing events ϕ. To determine the dependence of κ_H on ϕ, a series of runs was performed starting with the base run described above and varying ϕ to be either larger or smaller. The range of ϕ spanned one order of magnitude, with the base run falling approximately in the middle. A limiting factor in how small we could make ϕ was the model integration time; for example, to obtain a robust estimate of diffusivity for $(2\pi/f)\phi = 1.5 \times 10^{-4}$ we had to integrate for approximately 250 000 time steps, which on a dual 1-GHz processor Linux station took approximately 2.5 days. While this integration time is not prohibitive for any individual run, for the many different parameter dependencies we examined, plus the numerous control simulations (e.g., realistic f/N runs, higher resolution), the total number of runs and hence the total number of CPU hours was well over an order of magnitude larger than this. More important, however, is that the lower the event frequency and/or the higher the viscosity, the further our simulations get from reality in terms of the observed values of these parameters. Meanwhile, at the opposite extreme, that is, high event frequency and/or low viscosity, we encountered a different limitation, namely that simulations ceased to equilibrate to a statistically stationary state in which a meaningful estimate of diffusivity could be made (see below).

Results for κ_H versus ϕ are shown in Fig. 6. For small ϕ, κ_H varied approximately linearly with ϕ, consistent with (10) and (11). For larger ϕ, however, we observed a rapid increase in κ_H, indicating a transition to a more energetic, strongly nonlinear parameter regime. One symptom of this transition was the failure of model KE to equilibrate to a statistically stationary state. Since in those cases the rate of tracer dispersal depended on when the tracer was released, for large values of ϕ the meaning of κ_H was ill defined. We return to this more energetic regime in section 4f. Nevertheless, an importance conclusion, drawn from Fig. 6, is that, at least in the regime of interest (i.e., low ϕ), $\kappa_H \propto \phi$.

Viscosity (ν_2): We next examined the dependence of κ_H on viscosity ν_2. Again a series of runs was performed

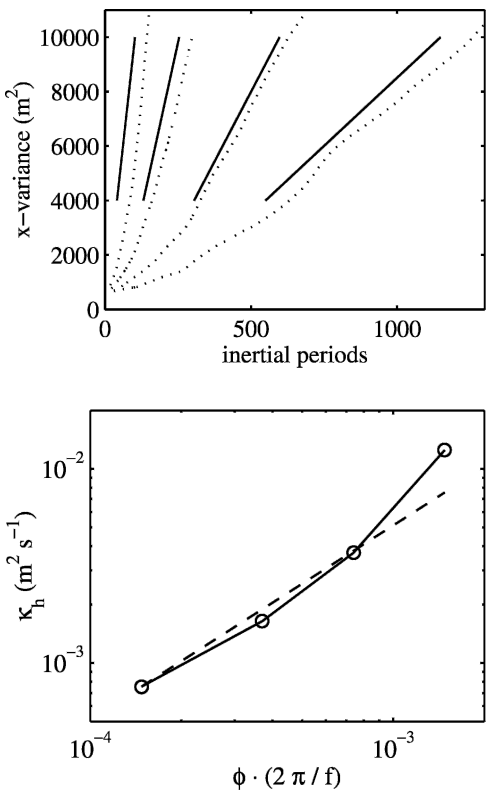

FIG. 6. (a) Growth of tracer variance and (b) effective lateral diffusivity κ_H caused by vortical mode stirring for a series of runs with varying frequency of mixing events ϕ. In (a) steeper slopes correspond to higher ϕ. In (b) the solid curves with circles indicate model results, while the dashed line indicates a linear dependence.

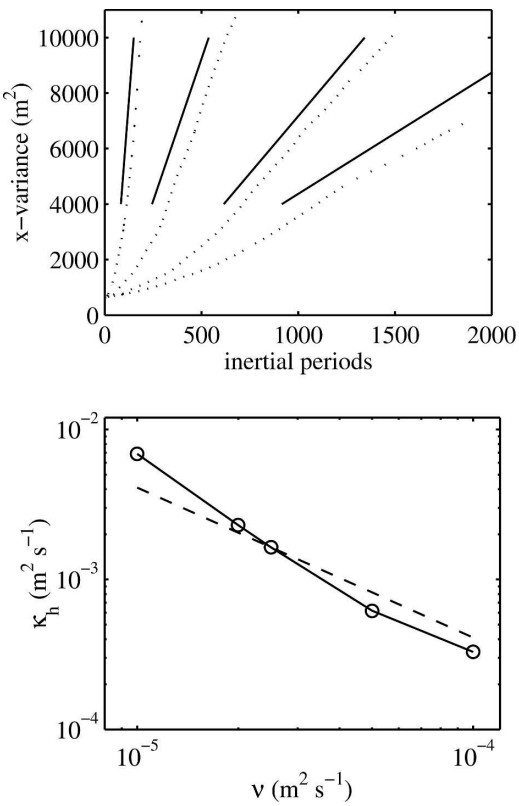

FIG. 7. (a) Growth of tracer variance and (b) effective lateral diffusivity κ_H caused by vortical mode stirring for a series of runs with varying Newtonian viscosity ν_2. In (a) steeper slopes correspond to lower ν_2. In (b) the solid curves with circles indicate model results, while the dashed line indicates a linear dependence.

starting with the base run, but this time varying ν_2. Again, the range spanned approximately an order of magnitude with the base run falling toward the high-viscosity end. Analogous to the case of low ϕ, a limiting factor for high values of viscosity was model integration time, while for low viscosity it was the failure of the model to equilibrate to a statistically steady state.

Results for κ_H versus ν_2 are shown in Fig. 7. For larger ν_2, we found an inversely linear dependence of κ_H, consistent with (10) and (11). For low ν_2 (high κ_H), however, again there was a transition to more energetic regime with much higher κ_H. As in the case of high ϕ, this transition corresponded to the failure of KE to equilibrate to a statistically stationary state. Nevertheless, at least for larger values of ν_2, we again conclude that the scaling given by (10) and (11) appears to be valid, that is, $\kappa_H \propto 1/\nu_2$.

Coriolis frequency and horizontal event scale (*f and L*): As noted above, the remaining parameter dependence of κ_H is somewhat more difficult to verify for a variety of reasons. Rather than examining each of the remaining parameters individually, we therefore examined them in concert, but still by comparing the results for κ_H with the predictions given by (10) and (11). Noting that R/L appears as a nondimensional parameter in (11), we began by examining f and L together so as to hold R/L, or alternatively the Burger and Rossby numbers, fixed.

As our first (f, L) run, we decreased f by a factor of 2 and increased L by a factor of 2 relative to our base run. If (10) holds, we would expect κ_H to increase by a factor of 2 since

$$\kappa_H \propto \left(\frac{1}{L^2}\right)\left(\frac{1}{f^3}\right).$$

Indeed our results showed that κ_H increased by a factor of 1.8.

As a second check of (f, L), we again decreased f by a factor of 2 and increased L by a factor of 2. However, this time, we also decreased viscosity, ν_2, by a factor of 2. In addition to the Burger and Rossby numbers, this also held the Ekman number fixed. If (10)

holds, we now would expect κ_H to increase by a factor of 4 since

$$\kappa_H \propto \left(\frac{1}{L^2}\right)\left(\frac{1}{f^3}\right)\left(\frac{1}{\nu_2}\right).$$

Again we found that our results were consistent with (10); specifically, κ_H increased by of a factor of 4.3.

As a final check of the dependence on (f, L), we performed a third run with f decreased by a factor of 2 and L increased by a factor of 2. This time, however, we additionally decreased both viscosity, ν_2, and the frequency of anomalies, ϕ, each by a factor of 2; that is, in addition to the Burger, Rossby, and Ekman numbers, we held the frequency of mixing events relative to the inertial time scale fixed. Here (10) would thus predict that κ_H should increase by a factor of 2, which it did. More important, however, as expected from the nondimensional form of the momentum equation (4), this run was nearly identical to the base run in terms of the energy, dye variance, and even the details of the vorticity and dye fields. (Note that in this case we also used the same random number seed for the anomalies as in the base run.) In other words, the two runs were dynamically similar after scaling the horizontal extent of anomalies with the deformation radius, and the viscous and anomaly recurrence time scales of events with the inertial time scale. This is consistent with similar findings for the adjustment of a single anomaly by LS, except in that case the frequency of anomalies was not a factor.

Buoyancy frequency and vertical event scale (N *and* h): To understand the dependence of κ_H on N and h, we note that these two parameters plus vertical viscosity and diffusion are the only parameters affecting vertical scales in the model. Furthermore, note that by varying N and h in concert (and indirectly, ΔN, since we hold $\Delta N^2/N^2$ fixed), we can again hold the deformation radius, R, and thus the Burger and Rossby numbers fixed. As a first test of the dependence on N and h, we therefore increased h by a factor of 2 and decreased N by a factor of 2. According to (10), this should lead to an increase in κ_H by a factor of 4. Instead, however, the model showed an unbounded growth in KE, similar to that described above for high ϕ and low ν_2.

We next repeated the same run, but this time we also increased the viscosity by a factor of 4. Based on (10), this should have resulted in the same κ_H as in the base run, which it did. Moreover, we found that the results of this run were again dynamically similar to our base run. This was again as expected from (4) since this choice of parameters preserves the Burger, Rossby, and Ekman numbers as well as the frequency of anomalies relative to the inertial time scale.

f. *Weakly nonlinear versus strongly nonlinear turbulent regimes*

Thus far, for low values of κ_H, the numerical results are consistent with the parameter dependence given by (10). However, for larger κ_H resulting, for example, from either high ϕ or low ν_2, we found that the model transitioned to a more energetic regime in which κ_H became very large. Closer inspection of these simulations suggests that, in these cases, strongly nonlinear vortical mode interactions led to a cascade of energy to larger scales and, hence, an unbounded growth of KE. To better understand this more energetic regime, we now briefly examine a simulation similar to our base run except that we have increased the frequency of mixing events, ϕ, by a factor of 10. The resulting run is typical of what we found in this strongly nonlinear turbulent regime.

Time series of PE and KE for the strongly nonlinear turbulent run are shown in Fig. 8. In contrast to the base run (see Fig. 2), model KE in the strongly nonlinear run did not equilibrate; rather, it continued to increase throughout the integration. Corresponding to this increase in total KE was a particularly large increase in the amount of energy at large scales. The latter was in turn accompanied by an increase in spectral slope at low wavenumbers from nearly zero in the base run to about k^{-3} in the strongly nonlinear case, and a decrease in spectral slope at intermediate wavenumbers from k^{-10} in the base run to k^{-5} in the strongly nonlinear case (Fig. 9, cf. with Fig. 3). Note-

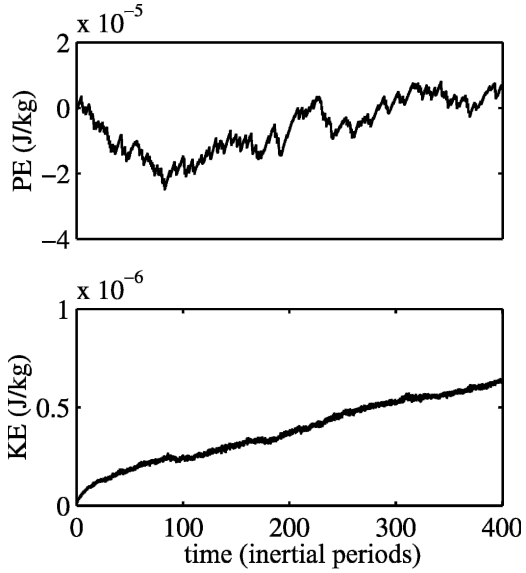

FIG. 8. Time series of (a) PE anomaly and (b) KE for the strongly nonlinear turbulent run showing unbounded growth in model KE (cf. with Fig. 2).

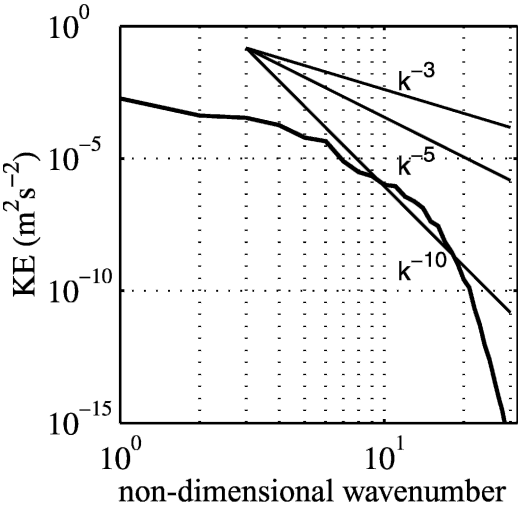

FIG. 9. Horizontal KE spectrum for a strongly nonlinear turbulent model run showing a k^{-5} spectral slope associated with an inverse energy cascade (cf. with Fig. 3). The rapid decrease of energy at large wavenumber (small scales) is due to the wavenumber truncation described above.

worthy is the similarity of these slopes to those reported by previous investigators in the context of two-dimensional turbulence without and with coherent structures, respectively (e.g., Basdevant et al. 1981; Bennett and Haidvogel 1983; Babiano et al. 1985; Maltrud and Vallis 1991). Such similarity is consistent with the quasi-two-dimensional (i.e., dominantly horizontal) nature of the velocity fields associated with the vortical mode (see also, LS).

Based on the above runs, as well as others not reported in detail here, we have found that the transition to the strongly nonlinear turbulent regime can be brought about by varying a number of different parameters. A condition that apparently precipitates this transition is that anomalies are densely populated in space and time, either by occurring very frequently or by lasting a long time, or both. Assuming that the transition threshold is related to the likelihood of encounters between individual vortices, we can estimate the approximate density of anomalies required to enable such interactions. At a minimum, we expect strongly nonlinear interactions to occur if the ratio of the viscous time scale to the recurrence time scale of events is greater than or equal to 1; if anomalies recur at a given location before preceding anomalies have had time to dissipate,

$$\frac{T_{\nu_B}}{1/\phi} = \left(\frac{h^2}{\nu_B}\right)\left(3\frac{N^2}{\Delta N^2}\frac{\kappa_z}{h^2}\right) = 3\frac{N^2}{\Delta N^2}\frac{\kappa_z}{\nu_B} \geq 1. \quad (20)$$

Here ν_B represents the background viscosity, which is presumed ultimately responsible for dissipating the anomalies, while κ_z is the net diapycnal diffusivity due to episodic mixing (see also Sundermeyer et al. 2005). Assuming $N^2/\Delta N^2 \sim 1$, this occurs when episodic mixing events contribute significantly to the overall diapycnal mixing, that is, when $\kappa_z \geq \nu_B$. Note that this condition does not imply that lateral stirring by small-scale vortices caused by the relaxation of mixed patches is insignificant, as evidenced by the results of the previous section.

Refining (20) somewhat, it can be shown on simple geometric grounds that strongly nonlinear interactions may occur, even before the above threshold is reached, since such interactions can also occur if anomalies are merely proximate to one another. In practice, we find from the above runs as well as others not described in detail here that strongly nonlinear interactions generally occur in our model for values of $\phi T_{\nu_B} \geq (0.01 - 0.1)$.

g. Some numerical checks

As final checks of the predicted parameter dependence and scaling, additional runs were performed to verify both the numerics and the scaling described above. The first of these checks was to examine the effect of our reduced N/f scaling, that is, the use of an artificially increased f in our model. To this end, we compared our base run with its unscaled (i.e., realistic f, L, and ν_2) analog; that is, we decreased f by a factor of 10 back to a realistic value of 9.5×10^{-4} s^{-1}, increased L by a factor of 10 to 500 m, decreased viscosity by a factor of 10 to 2.5×10^{-6} m^2 s^{-1}, and decreased the frequency of anomalies by a factor of 10. As described in the previous sections, this combination of parameter variations maintained fixed Burger, Rossby, and Ekman numbers and the frequency of events relative to the inertial frequency. As predicted by (4), the model fields were dynamically similar to the base run; that is, the two runs were nearly identical after scaling except for minor differences attributable to the internal wave field (see LS), provided we used the number of inertial periods as the time metric for comparison rather than some absolute measure, such as seconds or days. Moreover, as predicted by (10) and (11), the effective horizontal diffusivity κ_H increased tenfold relative to our base run.

As a second check, we verified that our choice of model resolution did not effect the model dynamics. To this end, we repeated our base run, but with double the vertical and horizontal grid resolution. As expected, the results were identical to our base run, suggesting that model resolution, indeed, did not affect our numerical solutions.

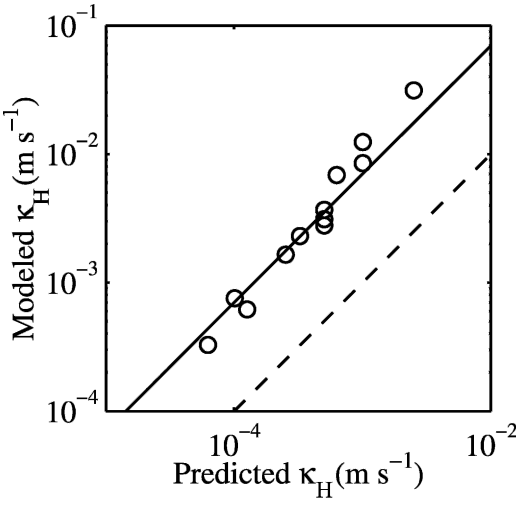

FIG. 10. Predicted vs modeled effective horizontal diffusivities for all model runs described in section 4e. The dashed line indicates 1:1 correspondence between predicted and modeled values, while the solid line is based on (10) times a constant scale factor of 7.

5. Discussion

a. Comparison with predicted scaling

The most significant finding of the present study is that model results were consistent with the theoretical scaling given by (10) and (11). Specifically, we found that for a wide range of forcing and viscosity/diffusion parameters, the effective horizontal diffusivity in the model agreed with the predicted scaling to within a constant scale factor. Based on the results of our numerical simulations, the value of this scale factor, which in the original scaling by Sundermeyer et al. (2005) was assumed to be of order 1, is actually about 7. Our results are summarized in Fig. 10, which shows the predicted versus modeled effective diffusivities for all runs described in section 4. The figure shows an approximately linear relationship between the predicted and modeled effective diffusivities that spans almost two orders of magnitude in κ_H. Thus, based on our simulations to date, we find that the scaling proposed by Sundermeyer et al. (2005) appears to be robust, at least in the weakly nonlinear regime.

As a caveat to the above, we note that, formally, our numerical results do not prove the scaling given by (10) and (11); rather, they merely demonstrate consistence with it. Figures 6 and 7 in particular make a strong case for the predicted dependence of κ_H on the frequency of events and the background viscosity. However, analogous plots showing the dependence on f, L, h, and N were not possible, partly because of the complexity of the parameter dependence of these variables, and partly because of computational/numerical limitations (see section 4e). As a result, our tests using different values of f, L, h, and N do not unambiguously show the dependence of these variables. For example, by decreasing f and increasing L, and obtaining the expected increase in κ_H, we have argued consistency with the dependence

$$\kappa_H \propto \left(\frac{1}{L^2}\right)\left(\frac{1}{f^3}\right)$$

in (10). However, the same change in κ_H could have resulted from a different parameter dependence, for example, if instead

$$\kappa_H \propto \left(\frac{1}{L^4}\right)\left(\frac{1}{f^5}\right).$$

The most conclusive evidence in support of the predicted scaling is that select combinations of the relevant parameters yielded solutions that were dynamically similar. Since the conditions for dynamical similarity are prescribed by (1)–(4) and since the theoretical scaling given by (10) and (11) is derived directly from these expressions, the effective horizontal diffusivity is constrained by the same dynamics.

Another important point regarding our model results is the implication of the reduced N/f scaling, that is, our use of an artificially increased value of f. As noted in section 3e, in all of our increased f runs, we also reduced L and increased ϕ and ν_2 by the same factor, that is, tenfold. The purpose of this was to hold the Burger, Rossby, and Ekman numbers fixed. One consequence of this, however, was that the effective lateral diffusivity by vortical mode stirring in our model was also reduced by a factor of 10, since according to (10),

$$\kappa_H \propto \left(\frac{1}{L^2}\right)\left(\frac{1}{f^3}\right)\left(\frac{\phi}{\nu_B}\right).$$

While this reduction in κ_H is consistent with the scaling (10) and (11), it also means that, in order to compare our model results with realistic ocean values, we must rescale the model κ_H by multiplying by 10 (or 5 in cases in which we decreased f by a factor of 2 relative to our base run). Doing this, we find that the values in Figs. 6, 7, and 10 correspond to realistic values of κ_H ranging from 10^{-2} to 10^{-1} m^2 s^{-1}.

The above values of κ_H, even after rescaling, are still considerably smaller than those observed during CMO. This is despite our use of realistic parameter values wherever possible to force the model. The reason for this is that, even after rescaling, all of our model simulations had a much lower frequency of mixing events ϕ and/or a (slightly) higher background viscosity ν_2 than occurs in the real ocean: The larger culprit here by far

was ϕ. Sundermeyer et al. (2005) estimated for CMO that the frequency of events at any given location was on the order of at least once per 3 days, or about one per four inertial periods (this assumes a vertical scale of $h = 1.25$ m). In contrast, the base run described in the previous section used a value of approximately one per 3000 inertial periods. The reason for this choice of ϕ was that for values larger than this the model became strongly nonlinear and, hence, effective horizontal diffusivities could not be unambiguously determined. This is a limitation of the simulations and scaling presented here.

Aside from ϕ, and in some cases ν_2, all other parameter values in the model were comparable to realistic values either directly observed or estimated during CMO. Nevertheless, given the unrealistically small value of ϕ used here, the exact relationship between the present simulations and the real ocean remains speculative. Extrapolating the predicted linear relationship between the frequency of events and the effective diffusivity, the scaling given by (10) and (11) suggests that the use of a realistic value of ϕ in our model would increase κ_H by three orders of magnitude. This would be more than enough to explain the observed κ_H during CMO. However, as described in section 4f, this scaling breaks down for large ϕ and/or small ν_2. Specifically, we have found that for values of

$$\frac{T_{\nu_B}}{1/\phi} \geq (0.01 - 0.1),$$

the dynamics in the model transition to a more energetic regime characterized by strongly nonlinear vortical mode interactions, and a cascade of energy to large scales. Thus, while the weakly nonlinear scaling may offer some insight, a comparable scaling for this strongly nonlinear turbulent regime is clearly needed.

b. Weakly nonlinear versus strongly nonlinear turbulent regimes

As noted above, in the absence of other factors, the cascade of energy to large scales and the concomitant unbounded growth of KE in our model lead to a much larger effective horizontal diffusivity than (10)–(11) predict. However, in the real ocean we speculate that such an energy cascade could not continue indefinitely; rather, at some scale it must eventually be arrested. In the open ocean, the Rhines arrest scale, determined by planetary β (e.g., Rhines 1975) limits the inverse energy cascade of geostrophic β-plane turbulence. This scale is likely too large to be of relevance over the continental shelf since it is generally comparable to the cross-shelf scale itself. However, in the coastal ocean other processes such as shearing or straining by large-scale internal waves or tides may arrest the cascade by limiting the effective horizontal and vertical scales of the vortical mode field and making it more prone to viscous dissipation. Preliminary model simulations of a single vortex superimposed on a low mode background internal wave fields suggest that, for sufficiently strong background shears, individual vortices are indeed effected. However, exactly how this affects the lateral diffusivity in the case of multiple vortices has not been examined.

One possible scenario for how the weakly and strongly nonlinear regimes may be related to one another and to the hypothesized energy arrest is shown schematically in Fig. 11. Here the transition between the two regimes is shown by a sharp increase in the effective lateral diffusivity at large ϕT_{ν_B}. However, there are many aspects of this picture that have yet to be verified, including the details of the transition from the weakly to strongly nonlinear regime, and the magnitude of the effective diffusivity in the strongly nonlinear regime. To make progress on these questions, future numerical studies will need to address the issue of energy buildup at large scales, in particular, whether to allow or remove such energy, and the realism of doing so.

c. A comment on R/L and geostrophic scaling

Regarding the parameter dependence given by (10) and (11), it is worth noting that the nondimensional parameter (R^2/L^2) indirectly contains an additional parameter dependence that is not accounted for by our scaling. Namely, as discussed by LS, the magnitude of the geostrophic velocity generated during the adjustment of a mixed patch depends on the precise value of R/L, not just its order of magnitude. In particular, LS found that for values of $R/L \geq 0.1$, but still ≤ 1.0, in general (5) overpredicts the actual vortex velocity that results in our model. For example, for $R/L = 0.4$ (the value used in our base run), the actual vortex velocity was about 3 times smaller than (5) would predict. While this difference does not have a major impact on our results, the difficulty that it presents in our dispersion analysis is that by varying L in our model runs, say from $L = R$ to $L = 2R$, geostrophic scaling implies that the velocity should decrease by a factor of 2, since $U \sim h^2\Delta N^2/Lf$. In fact, however, the actual adjustment velocity will change by somewhat less than this. This higher-order dependence has not been explicitly taken into account in (10) and (11), as these expressions simply assume geostrophic velocity scaling for $R/L \sim 1$. However, to avoid ambiguity and/or confusion in the results presented here, we have held R/L fixed in all of our runs, even as we varied other parameters in our model.

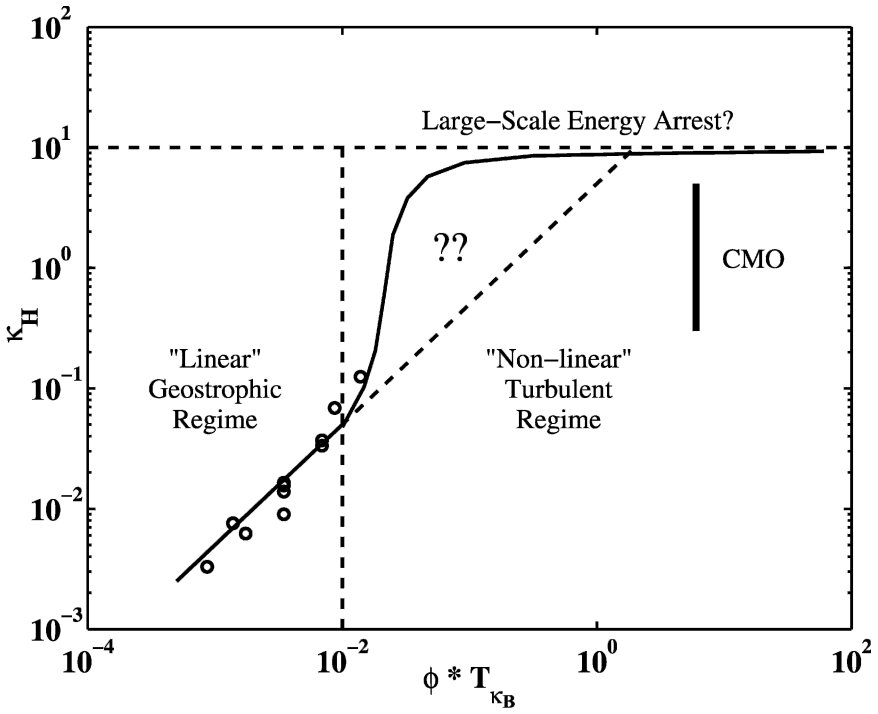

FIG. 11. Predicted effective horizontal diffusivity as a function of ϕT_{ν_B} for all model runs described in section 4e. Predicted values have been rescaled to realistic values based on N/f scaling. The transition to the strongly nonlinear regime described in the text is shown schematically along with the hypothesized energy arrest. Approximate values of ϕT_{ν_B} inferred from the CMO dye release experiments (see Sundermeyer et al. 2005) are also shown, along with the respective diffusivities.

Noteworthy, however, is that, had we used a different value of R/L in our simulations, we likely would have obtained a different value for the constant scale factor; that is, our inferred value of 7 is not necessarily universal among all values of R/L. Note that this is not an artifact of our numerical simulations, but rather is simply the nature of geostrophic adjustment. A more detailed examination of how the R/L dependence affects κ_H is left as a topic for future investigation.

d. An energy budget approach

An interesting implication of episodic (as opposed to uniform) diapycnal mixing is the simple fact that some of the PE generated by episodic diapycnal mixing events is converted back to KE through the process of geostrophic adjustment. As noted by Sundermeyer et al. (2005), in principle, it should thus be possible, with some assumptions, to estimate KE, and hence the effective horizontal diffusivity, κ_H, associated with the vortical mode field, directly from knowledge of the net buoyancy flux or, equivalently, the diapycnal diffusivity. We now consider this in some detail.

Consider a random field of isolated diapycnal mixing events as discussed in the previous sections. Classical adjustment theory suggests that, for a single axisymmetric lens, as much as half of the available PE (APE) may be released during geostrophic adjustment (e.g., Garrett 1984; McWilliams 1988; Arneborg 2002). The exact amount will depend on a variety of factors, including the scale of the initial anomaly relative to the deformation scale and the background dissipation rate. For example, an anomaly initially small relative to the deformation radius would lose a much higher percentage of its APE through adjustment than an anomaly that was initially of deformation scale. Of the energy released, previous studies have shown that between 30% and 50% will be converted to KE in the form of geostrophically balanced flow, while the remaining 50%–70% will go to generating internal waves, or be lost to dissipation (e.g., Ou 1986; McWilliams 1988). Indeed, LS have found that this balance bears out in numerical simulations of geostrophic adjustment of a single vortex.

In total, the above energy partition implies that up to 15%–25% of the available PE generated through diapycnal mixing may be converted back into KE in the

form of vortical modes. To determine the total KE of the vortical mode field at any given time, however, we also need to know the rate at which this APE is being supplied, as well as the decay time scale of the vortical mode field. Assuming we know the vertical scale of mixing events h, the frequency of events ϕ can be inferred from the net vertical diffusivity caused by the events via (8). Meanwhile, at least in the weakly nonlinear regime, the decay time scale, $T_{\nu_B} = h^2/\nu_B$, provides a measure of how long the individual geostrophic vortices will last. Following Sundermeyer et al. (2005), a rough estimate of the magnitude of the effective horizontal diffusivity can thus be obtained using the eddy diffusion formulation of Taylor (1921); that is,

$$\kappa_H \approx T_I \times \text{KE} \approx T_I \times (0.15 \text{ to } 0.25) \times (\text{production rate of APE}) \times T_{\nu_B}, \quad (21)$$

where (0.15–0.25) $\times$ production rate of APE $\times$ T_{ν_B} represents the amount of KE generated through geostrophic adjustment and the factor T_I represents the integral time scale of the motion. Assuming that the production rate of APE is given by the frequency of diapycnal mixing events, ϕ, times the APE of individual events,

$$\text{production rate of APE} = \phi\left(-\frac{2}{3}\rho_o \Delta N^2 h^3\right); \quad (22)$$

that the buoyancy flux associated with a mixing event can be expressed in terms of a diapycnal diffusivity per (8); and that the integral time scale T_I is of order the eddy turnover time, that is, a few inertial periods, and substituting into (21), it follows that the horizontal diffusivity should scale as

$$\kappa_H \approx (0.9\text{–}1.5)\left(\frac{N^2}{f^2}\right)\left(\frac{T_{\nu_B}}{1/f}\right)\kappa_z. \quad (23)$$

Noteworthy is the similarity between this result and (11); the differences being that here the factor R^2/L^2 is implicitly assumed to be of order 1 and the particular value of the constant scale factor.

6. Conclusions

In this study we examined lateral stirring by small-scale geostrophic motions, or vortical modes, generated by the adjustment of mixed patches following diapycnal mixing events. A major finding of this work is that the parameter dependence predicted by Sundermeyer et al. (2005) appears to be robust to within a constant scale factor for what we have termed the weakly nonlinear geostrophic regime. Specifically, for $R/L \sim 1$, the effective lateral diffusivity by vortical mode stirring is generally about 7 times that predicted by (10) and (11). We have confirmed a linear dependence of κ_H on the frequency of mixing events and an inverse linear dependence on the background viscosity, ν_B. In addition, based on a series of runs with varying L, h, f, and N, we have also found the model results to be consistent with the predicted parameter dependence for these variables. Last, we presented additional arguments for how similar scaling can be obtained directly from energetics considerations. Noteworthy is that the latter provide a means of relating the amount of energy, and hence the amount of stirring by the vortical mode field, directly to buoyancy production by turbulent kinetic energy.

A second major finding of this study is that there is an additional parameter regime that is not well described by the scaling of Sundermeyer (1998) and Sundermeyer et al. (2005) in which vortical mode stirring becomes even more energetic. This regime is characterized by strongly nonlinear vortical mode interactions and an energy cascade to large scales, which significantly enhance the effective lateral stirring by vortical modes. A key signature of this cascade is a characteristic k^{-3} to k^{-5} horizontal KE spectrum at low and intermediate wavenumbers similar to those reported by numerous investigators in the context of two-dimensional turbulence without and with coherent structures. Based on this and the overall agreement between the present results and the quasi-two-dimensional geostrophic/random walk model of Sundermeyer et al. (2005), we believe that vortical mode stirring in stratified waters shares many characteristics with two-dimensional turbulence.

The transition between the weakly nonlinear and strongly nonlinear turbulent regime in our model appears to be correlated with the level of nonlinear interactions between individual vortices. This transition can be brought about in a number of ways. We hypothesize that a necessary condition for the transition is that mixed patches must be densely populated, either by occurring very frequently or by lasting a long time, or both. As a rough approximation, we expect that strongly nonlinear interactions will occur if the ratio of the viscous time scale to the recurrence time scale of events is greater than or equal to 1, that is, if anomalies recur at a given location before preceding anomalies have had time to dissipate. Based on simple geometric grounds, we anticipate that strongly nonlinear interactions may occur even before the above threshold is reached. In practice, we have found that nonlinear vortical mode interactions occur in our model for values of $\phi T_{\nu_B} \geq (0.01 - 0.1)$.

As noted in our discussion, the strongly nonlinear

parameter regime, reported on only briefly here, is believed to be quite relevant to the real ocean. An interesting aspect of this strongly nonlinear regime is its inverse energy cascade, which in our numerical model leads to an unbounded buildup of energy at large scales. In the real ocean we hypothesize that there must be some mechanism that arrests this cascade and, hence, limits the dispersion. However, whether this is the case has not been thoroughly investigated and is the subject of ongoing study.

The existence of a strongly nonlinear turbulent regime for large values of ϕT_{ν_B}, and the fact that the CMO observations fell within that regime, means that we still cannot say conclusively whether vortical mode stirring can explain the dispersion observed during CMO. The most that we can assert is that extrapolation of the weakly nonlinear scaling into the strongly nonlinear regime implies that it can (see Fig. 11). However, we have already shown that these two regimes behave quite differently. Understanding the strongly nonlinear regime and any possible energy arrest is thus a critical next step toward understanding the dynamics of vortical mode stirring and how the vortical mode field is maintained in the real ocean. The present results for the weakly nonlinear regime are a first step toward that goal.

Acknowledgments. This work was supported by the Office of Naval Research under Grant N00014-01-1-0984 and HPCMP Conputational Project 2020 (ONRDC). The authors thank Kraig Winters for use of his numerical model. Also thanks are given to Jim Ledwell, Eric Kunze, Kurt Polzin, and Raffael Ferrari for many insightful discussions. Bill Smyth and an anonymous reviewer provided helpful suggestions during the review process.

REFERENCES

Arneborg, L., 2002: Mixing efficiencies in patchy turbulence. *J. Phys. Oceanogr.,* **32,** 1496–1506.

Babiano, A., C. Basdevant, and R. Sadourny, 1985: Structure functions and dispersion laws in two-dimensional turbulence. *J. Atmos. Sci.,* **42,** 941–949.

Basdevant, C., B. Legras, R. Sadourny, and M. Béland, 1981: A study of barotropic model flows: Intermittency, waves and predictability. *J. Atmos. Sci.,* **38,** 2305–2326.

Bennett, A. F., and D. B. Haidvogel, 1983: Low-resolution numerical simulation of decaying two-dimensional turbulence. *J. Atmos. Sci.,* **40,** 738–748.

Garrett, C., 1984: Turning points in universal speculation on internal waves. *A Celebration in Geophysics and Oceanography,* C. Garrett and C. Wunsch, Eds., Scripps Reference Series*,* Vol. 84, Scripps Institution of Oceanography, 38–46.

——, and W. Munk, 1972: Oceanic mixing by breaking internal waves. *Deep-Sea Res.,* **19,** 823–832.

Haynes, P. H., and M. E. McIntyre, 1987: On the evolution of potential vorticity in the presence of diabatic heating and frictional and other forces. *J. Atmos. Sci.,* **44,** 828–841.

Kunze, E., 2001: Waves: Vortical mode. *Encyclopedia of Ocean Sciences,* S. T. J. Steele and K. Turekian, Eds., Academic Press, 3174–3178.

Ledwell, J. R., A. J. Watson, and C. S. Law, 1998: Mixing of a tracer in the pycnocline. *J. Geophys. Res.,* **103,** 21 499–21 529.

——, T. F. Duda, M. A. Sundermeyer, and H. E. Seim, 2004: Mixing in a coastal environment: 1. A view from dye dispersion. *J. Geophys. Res.,* **109,** C10013, doi:10.1029/2003JC002194.

Lelong, M. P., and M. A. Sundermeyer, 2005: Geostrophic adjustment of an isolated diapycnal mixing event and its implications for small-scale lateral dispersion. *J. Phys. Oceanogr.,* **35,** 2352–2367.

Maltrud, M. E., and G. K. Vallis, 1991: Energy spectra and coherent structures in forced two-dimensional and beta-plane turbulence. *J. Fluid Mech.,* **228,** 321–342.

McWilliams, J. C., 1988: Vortex generation through balanced adjustment. *J. Phys. Oceanogr.,* **18,** 1178–1192.

Oakey, N. S., and B. J. W. Greenan, 2004: Mixing in a coastal environment: 2. A view from microstructure measurements. *J. Geophys. Res.,* **109,** C10014, doi:10.1029/2003JC002193.

Ou, H., 1986: On the energy conversion during geostrophic adjustment. *J. Phys. Oceanogr.,* **16,** 2203–2204.

Patterson, G. S., and S. A. Orszag, 1971: Spectral calculations of isotropic turbulence: Efficient removal of aliasing interactions. *Phys. Fluids,* **14,** 2538–2541.

Phillips, O. M., 1966: *Dynamics of the Upper Ocean.* 1st ed. Cambridge University Press, 261 pp.

Polzin, K. L., and R. Ferrari, 2004: Isopycnal dispersion in NATRE. *J. Phys. Oceanogr.,* **34,** 247–257.

Rhines, P. B., 1975: Waves and turbulence on a beta-plane. *J. Fluid Mech.,* **69,** 417–443.

Sundermeyer, M. A., 1998: Studies of lateral dispersion in the ocean. Ph.D. thesis, Massachusetts Institute of Technology–Woods Hole Oceanographic Institution Joint Program, 215 pp.

——, and J. F. Price, 1998: Lateral mixing and the North Atlantic Tracer Release Experiment: Observations and numerical simulations of Lagrangian particles and a passive tracer. *J. Geophys. Res.,* **103,** 21 481–21 497.

——, and J. R. Ledwell, 2001: Lateral dispersion over the continental shelf: Analysis of dye-release experiments. *J. Geophys. Res.,* **106,** 9603–9621.

——, ——, N. S. Oakey, and B. J. W. Greenan, 2005: Stirring by small-scale vortices caused by patchy mixing. *J. Phys. Oceanogr.,* **35,** 1245–1262.

Taylor, G. I., 1921: Diffusion by continuous movements. *Proc. London Math. Soc.,* **20A,** 196–212.

Vanneste, J., and P. H. Haynes, 2000: Intermittent mixing in strongly stratified fluids as a random walk. *J. Fluid Mech.,* **411,** 165–185.

Winters, K. B., J. A. MacKinnon, and B. Mills, 2004: A spectral model for processes studies of rotating, density stratified flows. *J. Atmos. Oceanic Technol.,* **21,** 69–94.